Applied Catalysis B: Environmental 144 (2014) 174–181

Contents lists available at ScienceDirect

Applied Catalysis B: Environmental

journal homepage: www.elsevier.com/locate/apcatb

Formation and growth of PbO_2 inside TiO_2 nanotubes for environmental applications

M. Cerro-Lopez [a,c], Y. Meas-Vong [c], M.A. Méndez-Rojas [b], C.A. Martínez-Huitle [d], M.A. Quiroz [a,*]

[a] Universidad de las Américas Puebla, Depto. Cs. Químico Biológicas, Lab. de Investigación en Electrocatálisis, Sta. Catarina Mártir s/n, Cholula 72810, Puebla, Mexico
[b] Universidad de las Américas Puebla, Depto. Cs. Químico Biológicas, Lab. de Nanotecnología, Sta. Catarina Mártir s/n, Cholula 72810, Puebla, Mexico
[c] Centro de Investigación y Desarrollo en Tecnología en Electroquímica, Parque Tecnológico Querétaro, 76703 Sanfandila, Pedro Escobedo Querétaro, Mexico
[d] Universidade Federal do Rio Grande do Norte, Centro de Ciencias Exatas, Depto. Química, Lagoa Nova – Natal 59056-400, RN, Brazil

ARTICLE INFO

Article history:
Received 21 February 2013
Received in revised form 11 June 2013
Accepted 3 July 2013
Available online 13 July 2013

Keywords:
Photoelectrocatalysis
TiO_2 nanotubes
PbO_2 deposits
Methyl red bleaching
Ti/TiO_2 NT-PbO_2 anodes

ABSTRACT

The electrodeposition of lead dioxide (PbO_2) in a Ti/TiO_2 nanotube (TiO_2 NT) array was achieved using a galvanostatic method at room temperature. The formation and growth of PbO_2 inside the TiO_2 NTs was followed as a function of the deposition time (t_d). The TiO_2 NT::PbO_2 (*x* s) samples, as well as the TiO_2 NTs previously prepared by anodization of Ti sheets, were characterized by scanning electronic microscopy (SEM) and X-ray diffraction (XRD) techniques. It was found that PbO_2 formation starts at the bottom of TiO_2 nanotubes and grows inside them until a well-dispersed deposit is achieved ($t_d \leq 5$ s) or until formation of PbO_2 crystalline deposits or cauliflower-like clusters outside the TiO_2 NTs at $t_d \geq 10$ s. In any case, the PbO_2 deposit always partially covered the TiO_2 NT arrays. Photochemical activity results showed that TiO_2 NT::PbO_2 (*x* s) samples had higher photocurrent density values than TiO_2 NTs. They also had better photoconversion efficiencies, which strongly suggest the occurrence of a photoelectro-synergistic effect due to electronic transfer assisted by the close contact between TiO_2 and PbO_2. This assumption was supported by the catalytic bleaching of methyl red (MR) dye solutions. Electrocatalytic (EC) and photoelectrocatalytic (PEC) results showed that, although the discoloration process is not entirely PEC dependent, its contribution is greater than the sum of the individual photocatalytic (PC) and EC processes, which confirms the synergic effect produced by the combination of TiO_2 and PbO_2 in a nanostructured array.

1. Introduction

In recent years, the photoelectrocatalytic degradation of organic pollutants as an advanced oxidation treatment (AOT) for water remediation has received special attention because it offers the possibility to combine the advantages of each technology to improve the overall process efficiency. Research has focused on developing materials that are capable of using UV–visible light to photogenerate active oxidizing species and have suitable electrochemical properties such as good conductivity and electroactivity toward oxidation. It is clear then that a sole material could not have all these desirable properties, but the combination of materials with appropriate properties may achieve this goal. Often, these composite materials for environmental applications are formed by a mixing process or by deposition of a photocatalytically active material on an electronic conductor substrate that exhibits suitable electrocatalytic properties. Variations on these combinations are also possible.

Titanium (Ti) has been used as a support for catalytically active metals for a long time because of its hardness, high conductivity, good chemical stability and adherence, and (mainly) to its low cost [1,2]. Ti self-generates an oxide layer that affects several of its properties, such as charge transport and ability to adhere deposits on its surface. However, the TiO_2 film has its own technical importance as protection from further corrosion or as an interface for physical–chemical processes, and particularly for its semiconductor properties. Under selected wavelengths, it may turn into a photoactive material with several uses, such as in a gas sensor [3–5], photocatalyst [6–8] or in dye-sensitized solar cells (DSC) [9,10]. However, the use of TiO_2 as an electrode material has been limited due to its poor electrocatalytic performance as an anode for organic compound electrooxidation.

Numerous studies to modify the structural and superficial characteristics of TiO_2 have been developed because of its potential

* Corresponding author.
E-mail address: marcoa.quiroz@udlap.mx (M.A. Quiroz).

0926-3373/$ – see front matter © 2013 Elsevier B.V. All rights reserved.
http://dx.doi.org/10.1016/j.apcatb.2013.07.018

uses to achieve (i) better chemical inertness, (ii) an increase of charge transport through the oxide layer, and (iii) better mechanical stability. Thus, it has been known for more than 40 years that by combining the effects of active and inert metal oxides, it is possible to obtain mixtures capable of increasing the catalytic properties, as observed for the $TiO_2 + RuO_2$ system [11–13]. In addition, since the rutile structure of RuO_2 is isomorphic with that of TiO_2, an improvement of its deposition and adhesion to the TiO_2 support is to be expected [14]. Indeed, the high miscibility between these oxides is due to their molar volumes being almost the same: $\delta(RuO_2) = 7.05\ g\ cm^{-3}$, $M(RuO_2) = 133.07\ g\ mol^{-1}$, therefore $V(RuO_2) = 133.07\ g\ mol^{-1}/7.05\ g\ cm^{-3} = 18.87\ cm^3\ mol^{-1}$; $\delta(TiO_2) = 4.25\ g\ cm^{-3}$, $M(TiO_2) = 79.90\ g\ mol^{-1}$, therefore $V(TiO_2) = 79.90\ g\ mol^{-1}/4.25\ g\ cm^{-3} = 18.80\ cm^3\ mol^{-1}$. Similar results have been reported previously for SiO_2 on TiO_2 [15].

On the other hand, lead dioxide PbO_2 is perhaps one of the most important oxides used in fundamental and applied electrochemistry [16]. PbO_2, in contrast to TiO_2, is a conductive metal oxide [17]. Since Thomas' work [18] on the electronic conductivity of PbO_2, it has been known that it ranges between $0.25 \times 10^4\ \Omega^{-1}\ cm^{-1}$ and $1.1 \times 10^4\ \Omega^{-1}\ cm^{-1}$, with a Hall coefficient between -1.7 and $-3.4\ cm^3\ A^{-1}\ s^{-1}$ and electron concentrations between 10^{20} and $10^{21}\ cm^{-3}$ [18–20]. In addition, from NMR data and ^{207}Pb chemical shift measurements on PbO_2, Rocard [21] and Frey [22] concluded that PbO_2 behaves like a metal in its electronic properties, i.e., it has metallic conductivity.

As an electrode, PbO_2 has been studied from its early use as the positive plate in the lead-acid battery until its current use as an anode in environmental applications. PbO_2 is considered as one of the most important anodic materials for the development of Advanced Oxidation Processes (AOPs). As an anode in aqueous media, PbO_2 exhibits a large overpotential for O_2 evolution (1.9 V/SHE [23]), allowing an effective production of active hydroxyl ($HO^{\bullet}$) radicals and consequently good performance for the oxidation of organic compounds. However, the traditional Pb/PbO_2 anode [24–27] does not have enough mechanical resistance, and the PbO_2 film corrodes in acidic media [28]. Therefore, other practical options for the preparation of PbO_2 anodes need to be considered. Different kinds of PbO_2 have been prepared: pure metal oxide [24–27], mixed with other metallic oxides [29], or doped with different ionic species [16,30–34]. Often, PbO_2 is deposited on a metallic substrate such as Ti [35,36], Au [37,38] or Pt [39,40] in order to improve its mechanical properties and to preserve its catalytic properties [28,41–43]. However, mechanical resistance and adherence problems between the Ti and the PbO_2 coating were observed, and the introduction of metallic transition layers was required to overcome such interfacial difficulties [29,35,44,45]. Thus, a particular type of anodic material called "modified titanium electrodes" has been developed; among these stand $Ti/TiO_2/PbO_2$ as dimensionally stable anodes (DSAs) [46–49]. The use of TiO_2 as a transition layer improves the corrosion resistance of Ti but not so the conductivity and other intermixed properties related to the PbO_2 deposit. This can be explained by the passive nature of the TiO_2 layer and because of the poor stability of the layer due to the low miscibility between TiO_2 ($18.8\ cm^3\ mol^{-1}$) and PbO_2 ($24.97\ cm^3\ mol^{-1}$). Nevertheless, deposition of PbO_2 on TiO_2 may be a good alternative to improve the photochemical properties of TiO_2 and to simultaneously take advantage of the electrocatalytic activity of PbO_2, as has recently been suggested by Li et al. [48] and Devilliers and Mahé [49].

Recently, a new type of interface consisting of TiO_2 nanotubes (TiO_2 NTs) has been developed by the anodic oxidation of pure Ti sheets in non-aqueous, fluoride-containing media [50–52]. These TiO_2 NT arrays are characterized by a compact structure of vertically aligned nanotubes, grown directly on the Ti surface, which provides an interfacial layer with a high surface area/volume ratio and an efficient electron transport in the metallic Ti substrate. Since the one-dimensional structure of the TiO_2 NT array reduces charge recombination, these interfacial nanostructured layers can be used as a matrix of enhanced photocatalytic activity [52–54] or as a support for other materials with surface activity, such as band-gap modifiers and electrocatalysts [55–62]. Such is the case of the electrochemical deposit of PbO_2 on TiO_2 NTs recently reported by Zhao et al. [63,64]. The authors used a nanotubular TiO_2 structure as an anchor for the PbO_2 deposit to form an electroactive layer of PbO_2 with better adherence and mechanical stability, consequently increasing by 3.5 times their life span with respect to Ti/PbO_2 anodes. Although these results are very promising in the direction of developing improved PbO_2 anodes, we suggest that the photoactivity of the TiO_2 NT array is meaningless due to the large amount of PbO_2 deposited into and on the TiO_2 NTs ($950.1\ g\ m^{-2}$ [63]), leading to a PbO_2 film whose thickness could probably be of several μm (Fig. 1b in [63]). If the interest is to develop an electrode material able to exhibit both electro (EC)- and photoelectro (PEC)-catalytic properties, then both TiO_2 and PbO_2 active sites must be exposed on the surface in contact with the electrolyte solution. Therefore, the goal of this work is to deposit and grow PbO_2 in a TiO_2 NT array in a controlled manner (partial coating) in order to expose both materials to the solution. Under those conditions, the material's photo-electroactivity is a consequence of a synergic mixing of the individual photo- and electro-activities. The results obtained will yield important information on the interfacial interactions between TiO_2 and PbO_2.

2. Experimental

2.1. Chemicals and reagents

Titanium (99.7%, 0.25 mm thick) and zirconium (99.8%, 0.125 mm thick) foils were purchased from Aldrich. Glycerol ($C_3H_8O_3$), sodium fluoride (NaF), sodium sulfate (Na_2SO_4), sulfuric acid (H_2SO_4), acetone (C_3H_6O), ethanol (C_2H_6O) and methanol (CH_4O) were also from Aldrich, all AR grade and used as received; deionized (DI) water was HPLC grade.

2.2. Preparation of vertically aligned TiO_2 nanotube (TiO_2 NT) interfaces

Titanium samples of $1\ cm^2$ were mechanically polished with no. 600 emery paper, 5 μm size alumina particles in water emulsion and ultrafine 3 μm abrasive paper, followed by a thorough rinse with DI water and degreasing by sequential ultrasonic cleaning in acetone, methanol and DI water for 10 min each and then blow dried with N_2 gas. After cleaning the Ti foil, TiO_2 NTs were prepared by anodization in a mixture of glycerol and DI water in a 1.3:1 ratio (v/v) containing 0.5 wt% NaF and 0.2 M Na_2SO_4 as a support electrolyte. A two-electrode electrochemical cell, with the electrodes separated by approximately 1 cm, was used with a Zr sheet as the counter electrode. Electrochemical anodization was carried out using a DC power supply (BK Precision model 1761) at an applied voltage of 20 or 30 V for 240 min. After anodic oxidation, the TiO_2 NTs were washed with DI water to remove the electrolyte and dried under a N_2 stream. Finally, the Ti/TiO_2 NT plate was annealed at 500 °C for 1.5 h in a tubular furnace with a heating rate of $5\ °C\ min^{-1}$ under air.

2.3. Deposition of lead dioxide

The electrodeposition of PbO_2 into the generated TiO_2 NT layer was carried out using a conventional three-electrode jacketed cell filled with a 0.25 M $Pb(NO_3)_2$ + 0.125 M HNO_3 solution

under a galvanostatic regimen (EG&G PAR Model 273 Potentiostat-Galvanostat) at an applied current density of 50 mA cm^{-2} (of geometrical area) during 5, 10 or 15 s of electrolysis time. The electronic arrangement was accomplished with an UHP graphite rod as the counter electrode and saturated mercury-mercurous sulfate (MSE: 0.616 V vs NHE) as the reference electrode. All electrolysis experiments were performed at a controlled temperature of 25 °C using a thermostated water bath (PolyScience model 9100).

2.4. Sample characterization

The morphologies of TiO_2 NTs and the PbO_2 deposits were determined by scanning electron microscopy (TESCAN VEGA model LSU) at a 20 kV accelerating voltage. The thickness of the nanotubular structures was examined in selected mechanically cut and cracked samples, and the elemental analysis was obtained using energy dispersive X-ray spectroscopy (EDAX, Oxford Ltd.). The crystalline phase of the TiO_2 NTs, as well as that of the PbO_2 deposits, was established with an X-ray diffractometer (DRX Bruker model D8Discover) using Cu Kα (λ = 1.54 Å) radiation.

The photocurrent responses of TiO_2 NTs and TiO_2::PbO_2 samples were obtained on a EG&G PAR Model 362 Scanning Potentiostat equipped with a model WX2400 Graphtec X-Y recorder, using a three-electrode jacketed cell specially designed to develop photochemical tests without reflection losses by windows. The Ti/TiO_2 NTs and Ti/TiO_2::PbO_2 electrodes were used as the photoanodes, Pt wire or UHP graphite rod as the counter electrode, and MSE (0.616 V vs NHE) as the reference electrode, although the potential data throughout the text were reported on the normal hydrogen electrode (NHE) scale. The photocurrent response variations of Ti/TiO_2 NTs and Ti/TiO_2 NT::PbO_2 electrodes with potential in 0.5 M H_2SO_4 were obtained by the linear scanning voltammetry (LSV) method at a slow potential sweep (5 mV s^{-1}). Experiments under controlled light illumination were carried out using a 100 W high-intensity long wave UV lamp (Blak-Ray model B 100AP), which produces 365 nm UV light of an irradiation intensity of 9.0 mW cm^{-2}, or a 6 W long wave lamp (Spectroline ENF-260C 6W) of intensity of 1.4 mW cm^2.

3. Results and discussion

3.1. Formation and characterization of TiO_2 NTs

TiO_2 NTs were prepared by anodic oxidation of Ti sheets previously polished and degreased to remove the organic contaminants on the Ti surface and also to provide a morphologically more homogeneous surface. Fig. 1 shows the nanotubular structure of TiO_2 obtained under the conditions previously indicated:

From Fig. 1a, it is possible to observe that the TiO_2 NT layer is a compact, disordered array of nanotubes with an average diameter of 100 nm and a length near 1 μm. Indeed, it is now well known that organization of nanotubes, as well as their dimensional parameters, is strongly dependent on the pretreatment previously applied to the Ti plates and the anodization conditions, including the chemical composition of the electrolysis bath. Highly ordered oxide nanotubes and uniform arrays can be produced on very smooth Ti surfaces, but when irregular Ti surfaces are used, non-uniform and disordered nanotube arrays are obtained. Nevertheless, the formation and growth mechanism of oxide nanotubes seems to be the same independent of whether or not the nanotube layer is an ordered array. Thus, it has been generally accepted that TiO_2 NT growth starts with the formation of a compact oxide layer induced by the presence of water in the electrolyte: $Ti + 2H_2O \rightarrow TiO_2 + 4H^+ + 4e^-$. In addition, the presence of fluoride ions in solution induces the chemical etching of the oxide: $TiO_2 + 6F^- + 4H^+ \rightarrow [TiO_6]^{2-} + 2H_2O$, and then the formation of small tubes is started [65,66].

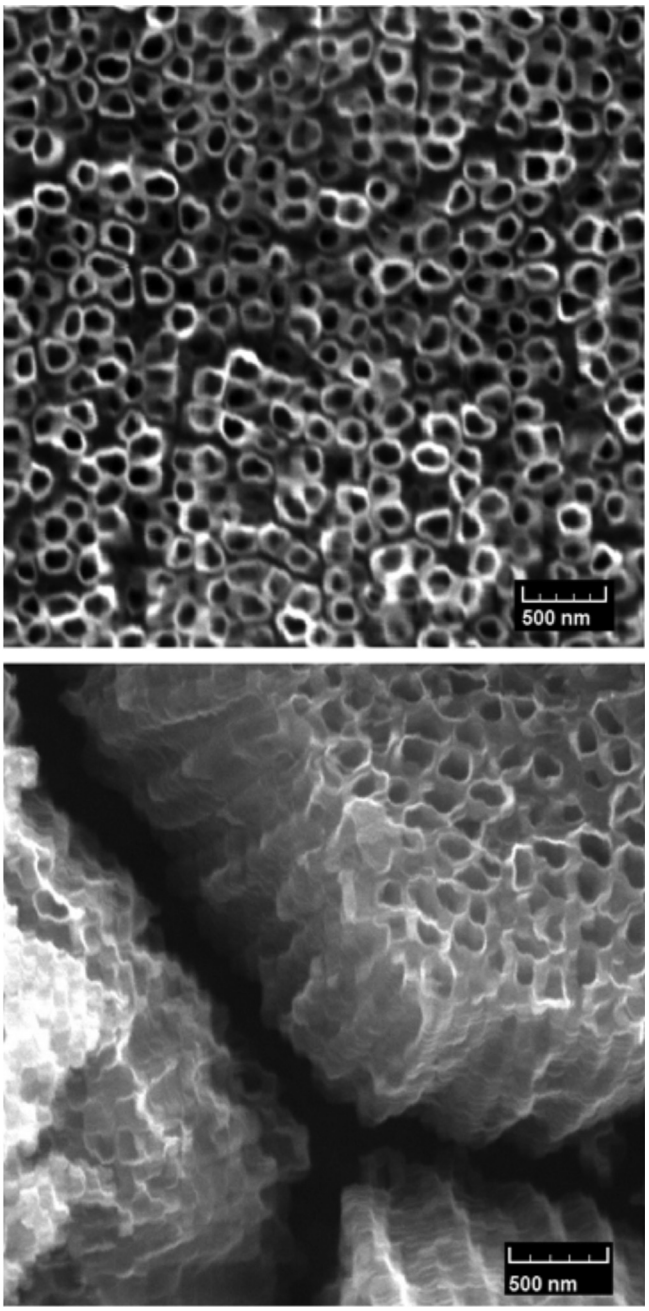

Fig. 1. SEM image of titanium anodized at 20 V for 2 h in a glycerol and DI water mixture of a 1.3:1 volumetric ratio containing 0.5 wt% NaF and 0.2 M Na_2SO_4. Ti/TiO_2 NT plates were annealed at 500 °C for 1.5 h with a heating rate of 5 °C min^{-1}. (a) top view; (b) cross-section.

The TiO_2 NT layer as formed has an amorphous structure which must be crystallized to an anatase crystal structure for practical purposes. Fig. 2 shows a XRD pattern of the TiO_2 NTs of Fig. 1a annealed at 500 °C for 1.5 h at a heating rate of 5 °C min^{-1}.

The XRD pattern of Fig. 2 clearly exhibits the diffraction peaks at 2θ = 25.3°, 37.1°, 37.9°, 38.5°, 48.1°, 53.9° and 55.1°, which can be assigned to the characteristic peaks of the anatase phase of TiO_2 (JCPDS No 89-4921). Complementary XRD peaks correspond to those characteristic and expected for the Ti substrate.

Once the morphology and chemical nature of the TiO_2 NT array were established, the photoactivity of TiO_2 NTs was evaluated by

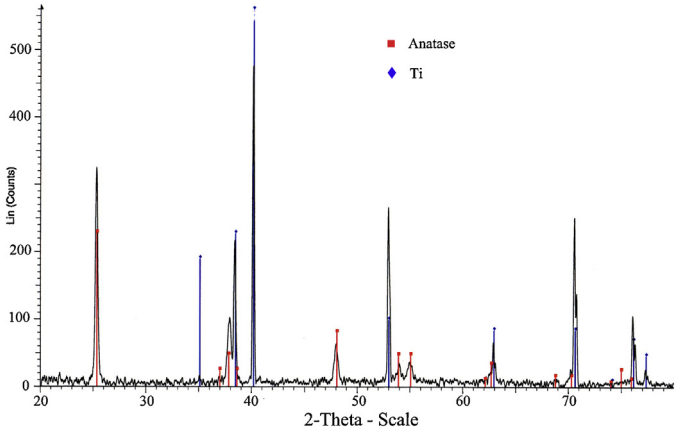

Fig. 2. XRD diffractogram of TiO_2 NT array after annealing at 500 °C for 1.5 h.

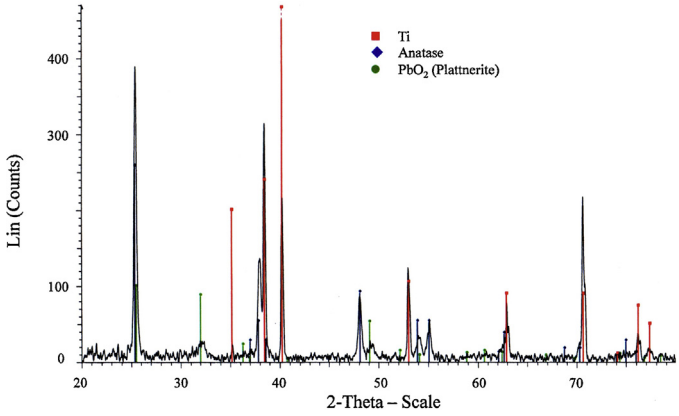

Fig. 4. XRD diffractogram for the PbO_2 deposit on TiO_2 NT array after 10 s of electrolysis time in a 0.25 M $Pb(NO_3)_2$ + 0.125 M HNO_3 solution.

photocurrent density measurements, which were obtained both in the dark and under UV light in an electrochemical setup that allowed both experiments in dark or light under the same electrochemical conditions. Fig. 3a shows the photocurrent density (j)–potential (E) curves of the Ti/TiO_2 NT electrode in 0.5 M H_2SO_4 solution, recorded within the potential range of 0.234 and 1.134 V vs NHE at a potential sweep rate of 5 mV s^{-1}:

As expected, the TiO_2 NT array exhibited higher photocurrent response compared with that under dark conditions, which is a clear sign of the semiconducting nature of the TiO_2 NT array and the occurrence of a typical n-type semiconductor/electrolyte junction characterized by the surface generation of electron–hole pairs [2]. As observed, as the bias potential shifts toward more positive values, the photocurrent response increases, which diminishes the electron–hole recombination and increases the photoelectron transfer efficiency of the TiO_2 NT array; this is the key factor of the photocatalytic properties of TiO_2-based electrodes. In this sense, the photoconversion efficiency (η) from light energy to chemical energy in the presence of a bias potential as calculated in [55,56] is shown in Fig. 3b. As observed, a maximum value of $\eta \sim 6.4\%$ was obtained at a minimal applied potential of 0.63 V vs NHE. Although this photoconversion efficiency seems small, it is comparable with those reported by Li et al. [56] and Quan et al. [55] for TiO_2 NTs of similar characteristics.

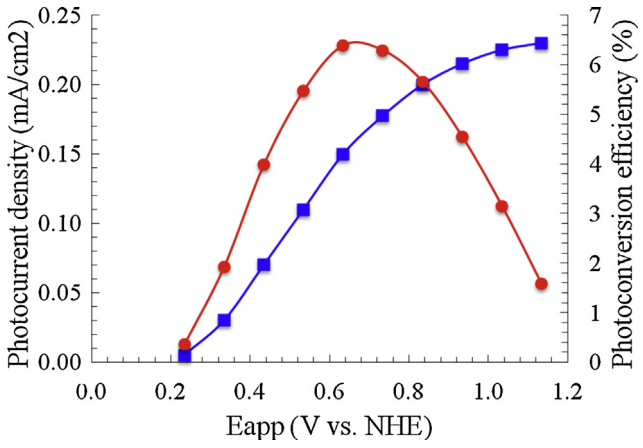

Fig. 3. (a) Photocurrent density (j) (blue squares) and (b) photoconversion efficiency (η) (red circles) as a function of the applied potential and with UV light illumination (365 nm) for a Ti/TiO_2 NT electrode in 0.5 M H_2SO_4. Sweep rate 5 mV s^{-1}; light power 1.4 mW cm^{-2}. (For interpretation of the references to color in this figure legend, the reader is referred to the web version of this article.)

3.2. Formation and growth of PbO_2 inside TiO_2 nanotube arrays

The inside of the nanotubular structure of TiO_2 is hydrophilic and therefore able to absorb liquid into the TiO_2 NTs when in contact with the aqueous phase. This wetting property allows the filling of the tubes with electrolytic solution and is the origin of the redox processes taking place in the TiO_2 NTs. Thus, the PbO_2 deposit from a $Pb(NO_3)_2$ solution can occur in the TiO_2 NTs in the same way as occurs on Ti, according to:

$$Pb^{2+}(ac) + 2H_2O(l) \rightarrow PbO_2(s) + 4H^+(ac) + 2e$$

The deposit of PbO_2 into the nanotubular structure of TiO_2 was confirmed by means of XRD and SEM analyses. Fig. 4 shows the XRD pattern for a PbO_2 deposit during 10 s on the TiO_2 NTs, which exhibits the characteristic peaks of the Plattnerite phase (β-PbO_2) in a tetragonal crystalline structure. The same XRD pattern indicates that the nanotubular structure of TiO_2 remains with that for PbO_2 and suggests that the latter is present in the bulk of the TiO_2 NT array inside the TiO_2 tubes, which was verified by SEM analysis.

The amount of PbO_2 deposited in the TiO_2 NT array can be controlled in a first instance by tuning the electrolysis time. In this case, the electrolysis time was fixed at 5, 10 and 15 s according to the experimental conditions described in Section 2.3. Fig. 5a–c shows the SEM images of these PbO_2 deposits:

SEM images show a large amount of PbO_2 on the surface of the TiO_2 NT layer as the electrolysis time increases but also indicate a change in the morphology of the PbO_2 deposited. In the first 5 s, the PbO_2 is formed inside the TiO_2 NTs without modifying its nanotubular structure. At 5 to 10 s, the amount of PbO_2 formed inside increases and overflows outside the nanotubular array, creating small PbO_2 crystals which, after some time, adopt a cauliflower-like crystalline shape. This crystal structure is favored at electrolysis times greater than 10 s, as observed in Fig. 5c. This growth behavior is strongly related to the electrolysis condition of PbO_2, the current density being the main factor to form PbO_2 deposits with high surface areas [34,67,68].

Although the formation and growth of PbO_2 inside the TiO_2 NTs is not appreciable from the top view SEM analysis, they can be observed from a side view. Fig. 6a displays a cross-bottom section obtained from a mechanically cracked sample of PbO_2 deposited at 10 s. Some pieces of this layer were lying upside down, which made the SEM observation easy.

Figs. 1 and 6a show that the TiO_2 nanotubes are open on the top, closed on the bottom and filled with PbO_2, in agreement with the data obtained from the XRD pattern of Fig. 4. The deposit of PbO_2 for only 15 s allows a dense but non-compact cauliflower-like PbO_2 layer to form, which allows access to exposed regions

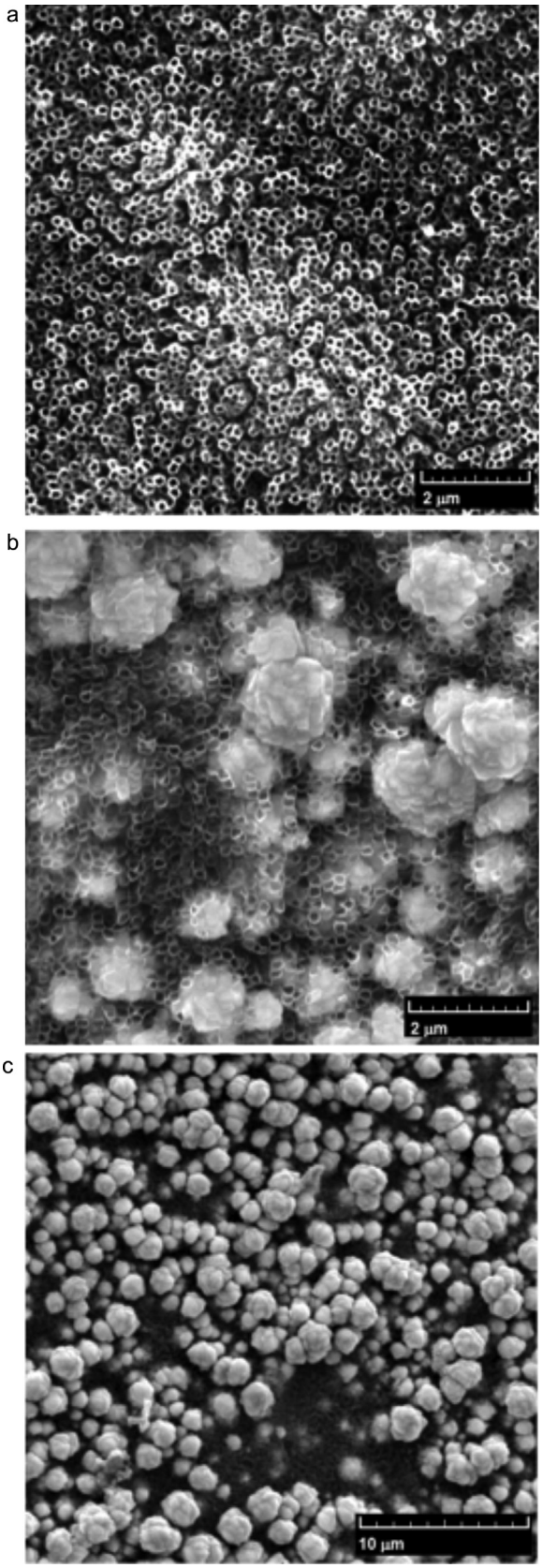

Fig. 5. SEM top view for of the PbO_2 coating on the TiO_2 nanotubular layer deposited from a 0.25 M $Pb(NO_3)_2$ + 0.125 M HNO_3 solution at an applied current density of 50 mA cm^{-2} (of geometrical area) during (a) 5, (b) 10 and (c) 15 s of electrolysis time.

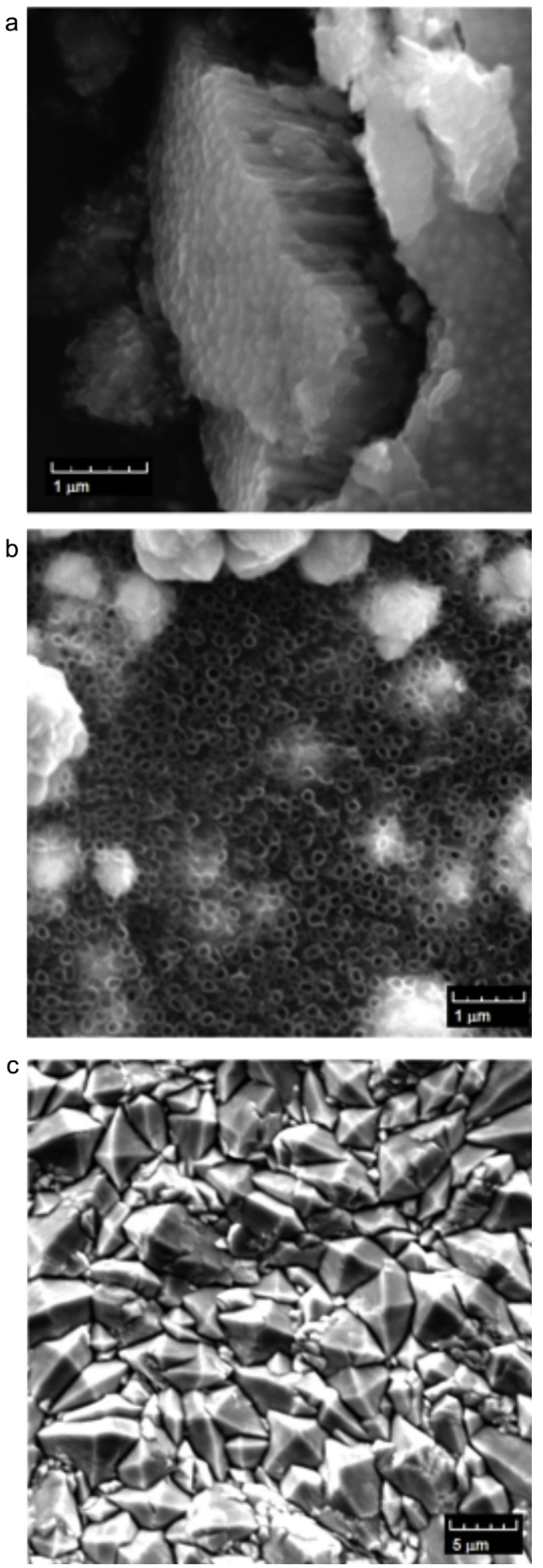

Fig. 6. (a) SEM side view for PbO_2 on a nanotubular TiO_2 layer which was mechanically cracked for observation. (b) Small region of TiO_2-NT::PbO_2 (15 s) of Fig. 5c magnified to observe the nanotubular structure of TiO_2 still present just under the cauliflower-shaped PbO_2 layer. (c) A massive PbO_2 deposit (35 min) on a TiO_2-NT substrate showing the characteristic tetrahedral crystal structure.

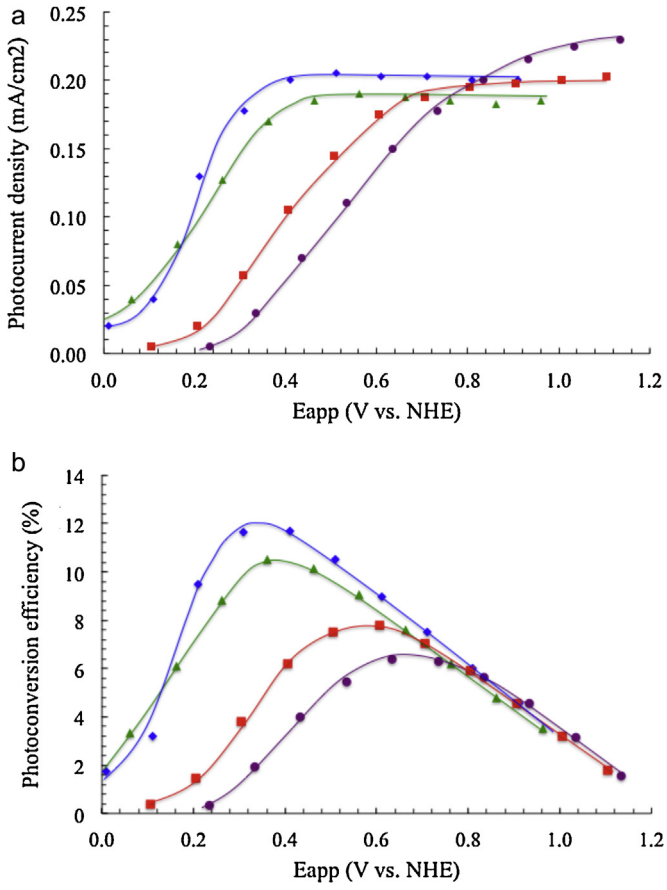

Fig. 7. (a) (left) Photocurrent density as a function of applied potential Eapp at TiO_2 NT and TiO_2 NT::PbO_2(x s) photoelectrodes under long wave UV light illumination (365 nm) in 0.5 M H_2SO_4. Sweep rate 5 mV s^{-1}; light power 1.4 mW cm^{-2}. Dark current densities were subtracted in order to remove the contribution of the applied potential.
(b) (right) Photoconversion efficiency (%) as a function of applied potential. Calculations are for: (purple circles) TiO_2 NTs, (blue diamonds) TiO_2 NTs::PbO_2(5 s), (red squares) TiO_2 NTs::PbO_2(10 s) and (green triangles) TiO_2 NTs::PbO_2(15 s).(For interpretation of the references to color in this figure legend, the reader is referred to the web version of this article.)

of TiO_2 NTs, as observed in Fig. 6b. That greatly differs from what has been observed for a massive PbO_2 deposit, as shown in Fig. 6c, which behaves as a typical PbO_2 material, characterized by a classic tetrahedral crystal structure.

The formation and growth of PbO_2 inside the nanotubular structure of TiO_2 is expected to modify the photochemical properties of TiO_2, as has been observed with other deposited species such as CdS quantum dots [69,60,70], noble metals [57,58], Sb-SnO_2 [56], Bi_2O_3 [59] and carbon nanotubes [71]. Therefore, in order to verify this assumption, photocurrent experiments were carried out for the previously prepared TiO_2 NT::PbO_2 samples, as shown in Figs. 5a–c. Fig. 7 indicates (a) the photocurrent density (mA cm^{-2}) and (b) the corresponding photoconversion efficiency (%) of the TiO_2 NT and TiO_2 NT::PbO_2 (5 s), TiO_2 NT::PbO_2 (10 s) and TiO_2 NT::PbO_2 (15 s) samples. It is important to point out that the values of photocurrent density represented in Fig. 7a do not include the dark current density, which, in some cases, is high due to the current contribution of PbO_2, a clearly non-photoactive species.

As can be observed in Fig. 7a, the photocurrent density increases with E_{app} until reaching a saturation value of about 0.20 mA cm^{-2} for all TiO_2 NT::PbO_2 (x s) samples, with a value slightly larger for TiO_2 NTs. These results suggest that growth of PbO_2 inside the TiO_2 NTs does not modify its band-gap energy, acting more like a metal with a strong interfacial interaction with TiO_2 than as a dopant, as is usual for other semiconducting materials. Since PbO_2 has a higher conductivity than TiO_2, it is expected that a high transport rate of electrons in the interface TiO_2::PbO_2 takes place, decreasing significantly the possibility for e^-–h^+ recombination. In addition, it is also observed in Fig. 7a that the flat band potential of TiO_2 NTs, estimated from the onset potential, was shifted toward more negative potential values for the TiO_2 NT::PbO_2 (x s) samples. The most negative flat band potential was observed for the TiO_2 NT::PbO_2 (5 s) sample, i.e., for the lower content of PbO_2 in TiO_2 nanotubes. These negative shifts of the flat band potential confirms our assumption of a low recombination rate of charged carriers and of the rise of a synergic effect which increases the photoconversion efficiency, as observed in Fig. 7b. Thus, Fig. 7b shows that the photoconversion efficiency for the TiO_2 NT::PbO_2 (x s) samples is higher than that observed for the empty nanotubes of TiO_2. It is also seen that in all cases, the maximum photoconversion efficiency was observed at applied potential values close to those of the photocurrent density saturation. These results strongly support the idea that the photochemical properties of TiO_2 are influenced by the presence of PbO_2 inside the nanotubes, an effect that increases as the quantity of PbO_2 decreases. As the amount of PbO_2 increases, the TiO_2 NT::PbO_2 (x s) layer is transformed into an essentially PbO_2 layer, as observed in Fig. 6c, which behaves as a typical metallic oxide without any photochemical property. These results are in agreement with the idea that the PbO_2 inside the TiO_2 nanotube arrays reaches a maximum superficial contact and then overflows outside the TiO_2 nanotubes, growing PbO_2 cauliflower-like clusters and switching off the TiO_2 photochemical properties. This explains the higher photoconversion efficiency (11.7%) observed for the TiO_2 NT::PbO_2 (5 s) sample, which presents the more negative value of flat band potential and the lowest chance of e^-–h^+ recombination. This photoconversion efficiency value is not as high as those measured with traditional doping species, which commonly change the band gap value as a consequence of a semiconductor::metal heterojunction, which creates a potential difference that impels the transport of photoelectrons across the TiO_2::PbO_2 interface and improves the photoelectric conversion efficiencies. Deposition times of PbO_2 higher than 5 s decreases the photoconversion efficiency, as observed in Fig. 7b, due to the effect of nucleation and formation of PbO_2 cauliflower-like structures which improve the electrical conductivity but avoid the incidence of UV light to the photoactive sites of TiO_2.

3.3. *Electrocatalytic (EC) and photoelectrocatalytic (PEC) bleaching of methyl red (MR) dye solutions*

Previously, it was discussed that the TiO_2 NT::PbO_2 (x s) samples have a higher photoconversion efficiency than that corresponding to uncovered TiO_2 NTs, which suggests that the PEC reactions may be improved with respect to the TiO_2 NTs and also to those occurring on classical Pb/PbO_2 or Ti/PbO_2 anodes. Therefore, with the aim to verify this last assumption, we evaluated the PEC activity for the TiO_2 NT::PbO_2 (5 s) sample (Fig. 5) in the bleaching of a MR dye solution under dark and UV light irradiation conditions. Fig. 8 presents a plot of the dependence of the EC and PEC discoloration of MR dye solutions on the electrolysis time in 0.5 M H_2SO_4 + 25 ppm MR dye solutions at 30 mA cm^{-2} with magnetic stirring and at room temperature. Color decay of the MR dye solutions was followed by absorbance measurements at a wavelength of 525 nm, as shown in Fig. 8. In dark conditions, the TiO_2 NT anode (empty red symbol) shows a low percentage of discoloration after 120 min of electrolysis, which is clearly negligible compared to the results obtained when using TiO_2 NT::PbO_2 (5 s) anodes (empty blue symbol) at the same dark conditions. These results support the idea that the catalytic activity of the TiO_2 NT::PbO_2 (5 s) anode is essentially of the EC type and favored by the generation of $HO^\bullet$ radicals on the PbO_2

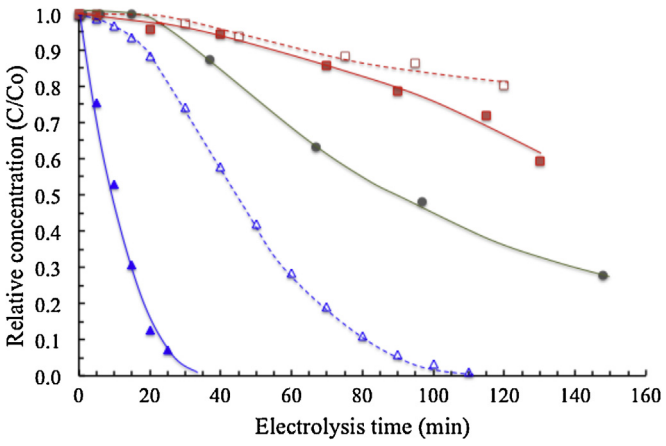

Fig. 8. Variation of MR relative concentrations with electrolysis time on different anodes (TiO_2 NTs::PbO_2 (5 s), blue triangles; TiO_2 NTs, red squares; and Pb/PbO_2, black circles). Current density = 30 mA cm^{-2}, [MR]0 = 25 ppm, supporting electrolyte = 0.5 M H_2SO_4, at room temperature. Empty symbols for dark conditions and filled symbols under UV light (365 nm) illumination conditions. The wavelength for absorbance measurements was 525 nm.(For interpretation of the references to color in this figure legend, the reader is referred to the web version of this article.)

active sites. The higher EC activity of the TiO_2 NT::PbO_2 (5 s) anode regarding that observed for the Pb/PbO_2 anode (filled black symbol) should be essentially due to a surface exposed area factor, favoring rapid changes in absorbance indicating that oxidation of this dye to other more simple organic compounds occurs by chromophore group breaking.

The more interesting aspect to observe in Fig. 8 is that on the TiO_2 NT::PbO_2 (5 s) anode under UV light illumination (filled blue triangles), the relative MR concentration drastically decreases after 20 min of electrolysis, but under dark conditions (empty blue triangles), color disappears only after 110 min. This fact clearly demonstrates that irradiation condition is a key factor for accelerating the discoloration process of the MR dye solution on the TiO_2 NT::PbO_2 (5 s) anode. In this sense, we can propose that the observed PEC activity for this last anode is due to a synergic effect and not only to a simple addition of catalytic contributions, that is, the simultaneous photochemical contribution by the TiO_2 NTs and the electrochemical contribution of the PbO_2 deposit. As previously said, applying a positive potential to the flat band potential of the TiO_2 NT::PbO_2 (5 s) anode minimizes the chances of recombination of e^- and h^+, which leads to an increase of the PEC efficiency. Considering that the bleaching process of the MR dye solution was carried out at 30 mA cm^2, which results in an oxidation potential of 2.97 V vs NHE, the TiO_2 NT::PbO_2 (5 s) anode should exhibit the best PEC oxidation ability, as shown in Fig. 8. Therefore, it is proposed that the synergic effect showed by the TiO_2 NT::PbO_2 (5 s) anode may be explained as follows.

The PbO_2::TiO_2::electrolyte system has two important interfaces: PbO_2::TiO_2 and TiO_2::electrolyte, creating on each a gradient of potential which stimulates electron transfer by two different charge carriers. In the first case, when PbO_2 is formed inside the TiO_2 NTs, the differences in conductivity yield an electrochemical gradient of potential in the heterojunction, which is able to improve the electron transfer through the TiO_2::PbO_2 interface, increasing the photoconversion efficiency. In the second case, the potential gradient generated by the TiO_2::electrolyte junction stimulates the hole transfer into the interface. When an external potential is applied under UV light irradiation conditions, the potential gradient increases in such grade that it yields a complete separation of the charge carriers (depletion condition). The photo-generated electrons are now efficiently transported into the PbO_2::TiO_2 interface, and from there to the cathode following the sequence:

$$VB(TiO_2) \rightarrow CB(TiO_2) \rightarrow LEO(PbO_2) \rightarrow bulk(TiO_2) \rightarrow substrate(Ti) \rightarrow cathode(C)$$

where VB and CB represent the valence and conduction bands of TiO_2, LEO the lower energy orbital of PbO_2 and the remaining the typical interpretation for TiO_2, Ti and carbon auxiliary electrodes.

On the other hand, the occurrence of this assisted electronic transfer by the close contact between TiO_2 and PbO_2 also yields an important opposite flow of holes toward the TiO_2::electrolyte interface, where they are involved in the oxidation of water to form free $HO^\bullet$ radicals or the direct oxidation of the MR dye, depending on the oxidation potential fixed by the applied current density. Additionally, it should be noted that PbO_2 anodes exhibit good electrocatalytic properties toward the oxidation of organic molecules due to the interactions between Pb(IV) sites and active groups of the organic pollutant, in this case MR. This mechanism favors the rapid oxidation of organic pollutants in solution, as previously reported by Bonfatti et al. [72], Martinez-Huitle et al. [73,74] and Ferro et al. [75]. In addition, this material offers reasonable service life and resistance to deterioration by the characteristic feature in its preparation (see Supplementary Material). However, it is important to consider that the global process is not restricted only to PEC or PbO_2 material, but is the main contributor with respect to the contributions of the individual photo- and electro-processes [76].

4. Conclusions

PbO_2 can be formed and grown inside TiO_2 vertically aligned nanotube arrays by a galvanostatic method. The amount of PbO_2 electrodeposited depends on the electrolysis time. In the first 15 s of electrolysis time, the SEM analysis shows that a TiO_2::PbO_2 array is formed by the close contact between a *n*-type semiconductor (TiO_2 nanotube) and a conductive metallic oxide (PbO_2). As anode, the Ti/TiO_2 NT::PbO_2/electrolyte array yields two types of active interfaces which play an important role in the photoconversion efficiency. Photochemical results showed that the TiO_2 NT::PbO_2 (5 s) sample exhibits the most negative flat band potential and consequently the lower possibility of recombination of charge carriers (e^-–h^+). These photochemical characteristics give that sample the best photoconversion efficiency (11.7%), as the applied potential becomes more positive (0.41 V vs NHE) than that of the corresponding flat band potential (0.01 V vs NHE). This latter photoconversion efficiency value (11.7%) is almost the double of the value obtained for the TiO_2 NT anode (6.2%) at the minimum applied potential of 0.63 V vs NHE, which is a remarkable result considering that PbO_2 is not a doping specie that may modify the band gap of TiO_2. In addition, the same TiO_2 NT::PbO_2 (5 s) anode showed the best photoelectrocatalytic (PEC) performance in the bleaching process of a MR dye solution. These results allow us to conclude that, although the discoloration process is not entirely PEC dependent, its contribution is greater than the sum of the individual photocatalytic (PC) and electrocatalytic (EC) processes, which confirms the synergic effect produced by the combination of TiO_2 and PbO_2 in a nanostructured array.

Acknowledgments

This work was supported jointly by the Consejo Nacional de Ciencia y Tecnología (CONACYT) México (Project No. 156200 CB-2010-01) and Dirección de Investigación y Posgrado from VA-UDLAP, México (Convocatoria 2012).

Appendix A. Supplementary data

Supplementary data associated with this article can be found, in the online version, at http://dx.doi.org/10.1016/j.apcatb.2013.07.018.

References

[1] B. Correa-Lozano, Ch. Comninellis, A. De Battisti, Journal of Applied Electrochemistry 26 (1996) 683.
[2] M. Neumann-Spallart, Chimia 61 (2007) 806.
[3] A. Telcki, N. Bjelobrk, S.E. Pratsinis, Sensors and Actuators B 130 (2008) 449.
[4] I.D. Kim, A. Rothschild, D.J. Yang, H.L. Tuller, Sensors and Actuators B 130 (2008) 9.
[5] O.K. Varghese, D. Gong, K.G. Ong, C.A. Grimes, Sensors and Actuators B 93 (2003) 338.
[6] Z. Ding, G.Q. Lu, P.F. Greenfield, Journal of Physical Chemistry B 104 (2008) 4815.
[7] J.L.G. Fierro (Ed.), Metal Oxides: Chemistry and Applications, CRS Taylor & Francis, Berkely California, 2006.
[8] T. Minabe, D.A. Tryk, P. Sawunyama, Y. Kikuchi, K. Mashimoto, A. Fujishima, Journal of Photochemistry and Photobiology 137 (2000) 53.
[9] J.Y. Kim, S.H. Kim, H.H. Lee, K. Lee, W. Ma, X. Gong, A.J. Heeger, Advanced Materials 18 (2006) 572.
[10] A. Mills, G. Hill, S. Bhopal, I.P. Pakin, S.A. O'Neill, Journal of Photochemistry and Photobiology 160 (2003) 185.
[11] A. Gerrard, B.C.H. Steele, Journal of Applied Electrochemistry 8 (1978) 417.
[12] V.I. Bystrov, V.V. Avksentyev, V.A. Sokolov, Zhurnal Fizicheskoi Khimii 47 (1973) 2561.
[13] I.E. Veselovskaya, E.K. Spasskaya, V.A. Sokolov, V.I. Tkachenko, L.M. Yakimenko, Elektrokhimiya 10 (1974) 70.
[14] S. Trasatti, G. Lodi, in: S. Trasatti (Ed.), Electrodes of Conductive Metallic Oxides, Part A, Elsevier, Amsterdam, 1989 (Chapter 7).
[15] G. Lodi, C. Bighi, C. De Asmundis, Materials Chemistry 1 (1976) 177.
[16] X. Li, D. Pletcher, F.C. Walsh, Chemical Society Reviews 40 (2011) 3879.
[17] J.P. Carr, N.A. Hampson, Chemical Reviews 72 (1972) 679.
[18] U.B. Thomas, Journal of the Electrochemical Society 94 (1948) 42.
[19] W. Mindt, Journal of the Electrochemical Society 116 (1969) 1076.
[20] F. Lappe, Journal of Physics and Chemistry of Solids 23 (1962) 1563.
[21] J.M. Rocard, M. Bloom, L.B. Robinson, Canadian Journal of Physics 37 (1959) 522.
[22] D.A. Frey, H.E. Weaver, Journal of the Electrochemical Society 107 (1960) 930.
[23] M. Panizza, G. Cerisola, Chemical Reviews 109 (2009) 6541.
[24] H.S. Awad, N. Abo Galwa, Chemosphere 61 (2005) 1327.
[25] M.A. Quiroz, S. Reyna, C.A. Martínez-Huitle, S. Ferro, A. De Battisti, Applied Catalysis B: Environmental 59 (2005) 259.
[26] H. Karami, A. Yaghoobi, A. Ramazani, International Journal of Electrochemical Science 5 (2010) 1046.
[27] C.A. Martínez-Huitle, A. De Battisti, S. Ferro, S. Reyna, M. Cerro-López, M.A. Quiroz, Environmental Science and Technology 42 (2008) 6929.
[28] J. González-García, J. Iniesta, E. Expósito, V. García-García, V. Montiel, A. Aldaz, Thin Solid Films 352 (1999) 49.
[29] F. Hine, M. Yasuda, T. Iida, Y. Ogata, K. Hara, Electrochimica Acta 29 (1984) 1447.
[30] I.H. Yeo, D.C. Johnson, Journal of the Electrochemical Society 134 (1987) 1973.
[31] J. Feng, L.L. Huok, D.C. Johnson, S.N. Lowery, J.J. Carey, Journal of the Electrochemical Society 142 (1995) 3626.
[32] J. Cao, H. Zhao, F. Cao, J. Zhang, C. Cao, Electrochimica Acta 54 (2009) 2595.
[33] A.B. Velichenko, R. Amadelli, E.A. Baranova, D.V. Girenko, F.I. Danilov, Journal of Electroanalytical Chemistry 527 (2002) 56.
[34] Y. Mohd, D. Pletcher, Journal of the Electrochemical Society 152 (2005) D97.
[35] M. Ueda, A. Watanabe, T. Kameyama, Y. Matsumoto, M. Sekimoto, T. Shimamune, Journal of Applied Electrochemistry 25 (1995) 817.
[36] G. Cifuentes, L. Cifuentes, R. Kammel, J. Torrealba, A. Campi, Zeitschrift fur Metallkunde 89 (1998) 363.
[37] A.B. Velichenko, D.V. Girenko, F.I. Danilov, Journal of Electroanalytical Chemistry 405 (1996) 127.
[38] Ch. Comninellis, E. Plattner, Journal of Applied Electrochemistry 12 (1982) 399.
[39] A.B. Velichenko, R. Amadelli, A. Benedetti, D.V. Girenko, S.V. Kovalyov, F.I. Danilov, Journal of the Electrochemical Society 149 (2002) C445.
[40] D. Devilliers, M.T.D. Thi, E. Mahe, Q. Le Xuan, Electrochimica Acta 48 (2003) 4301.
[41] J. Lee, H. Varela, S. Uhm, Y. Tak, Electrochemistry Communications 2 (2000) 646.
[42] Y.J. Feng, X.Y. Li, Water Research 37 (2003) 2399.
[43] D.J. Gilroy, Journal of Applied Electrochemistry 12 (1982) 181.
[44] M.H. Zhou, Q.Z. Dai, L.C. Lei, C. Ma, D.H. Wang, Environmental Science and Technology 39 (2005) 363.
[45] J.H. Wang, K.L. Lee, Journal of Applied Electrochemistry 26 (1996) 153.
[46] C. Comninellis, Electrochimica Acta 39 (1994) 1857.
[47] G. Foti, C. Mousty, V. Reid, C. Comninellys, Electrochimica Acta 44 (1998) 813.
[48] J. Li, L. Zheng, L. Li, G. Shi, Y. Xian, L. Jin, Electroanalysis 18 (2006) 2251.
[49] D. Devilliers, E. Mahé, Electrochimica Acta 55 (2010) 8207.
[50] L.V. Taveira, J.M. Macak, H. Tsuchiya, L.F.P. Dick, P. Schmuki, Journal of the Electrochemical Society 152 (2005) B405.
[51] J.M. Macak, P.J. Barczuk, H. Tsuchiya, M.Z. Nowakowska, A. Ghicov, M. Chojak, S. Bauer, S. Virtanen, P.-J. Kulesza, P. Schmuki, Electrochemistry Communications 7 (2005) 1417.
[52] X. Quan, S.G. Yang, X.L. Ruan, H.M. Zhao, Environmental Science and Technology 39 (2005) 3770.
[53] H.-F. Zhuang, C.-J. Lin, Y.-K. Lai, L. Sun, J. Li, Environmental Science and Technology 41 (2007) 4735.
[54] S. Yuan, L. Yu, L. Shi, J. Wu, J. Fang, Y. Zhao, Catalysis Communications 10 (2009) 188.
[55] X. Quan, S. Yang, X. Ruan, H. Zhao, Environmental Science and Technology 39 (2005) 3770.
[56] P. Li, G. Zhao, X. Cui, Y. Zhang, Y. Tang, Journal of Physical Chemistry C 113 (2009) 2375.
[57] M. Hosseini, M.M. Momeni, M. Faraji, Journal of Molecular Catalysis A: Chemical 335 (2011) 199.
[58] H. Yu, X. Wang, H. Sun, M. Huo, Journal of Hazardous Materials 184 (2010) 753.
[59] X. Zhao, H. Liu, J. Qu, Applied Surface Science 257 (2011) 4621.
[60] Y. Zhang, G. Zhao, Y. Lei, P. Li, M. Li, Y. Jin, B. Lv, ChemPhysChem 11 (2010) 3491.
[61] S. Chen, M. Paulose, C. Ruan, G.K. Mor, O.K. Varghese, D. Kouzoudis, C.A. Grimes, Journal of Photochemistry and Photobiology A: Chemistry 181 (2006) 177.
[62] D.R. Beker, P.V. Kamat, Journal of Physical Chemistry C 113 (2009) 17967.
[63] G. Zhao, Y. Zhang, Y. Lei, B. Lv, J. Gao, Y. Zhang, D. Li, Environmental Science and Technology 44 (2010) 1754.
[64] Y. Lei, G. Zhao, Y. Zhang, M. Liu, L. Liu, B. Lv, J. Gao, Environmental Science and Technology 44 (2010) 7921.
[65] H. Habazaki, K. Fushimi, K. Shimizu, P. Skeldon, G. Thompson, Electrochemistry Communications 9 (2007) 1222.
[66] W. Chanmanee, A. Watcharenwong, C.R. Chenthanmarakshan, P. Kajitvichyanukul, N.R. de Tacconi, K. Rajeshwar, Journal of the American Chemical Society 130 (2008) 965.
[67] P.K. Shen, X.L. Wei, Electrochimica Acta 48 (2003) 1743.
[68] Y. Mohd, Journal of Science and Technology 3 (2011) 109.
[69] W.T. Sun, Y. Yu, H.Y. Pan, X.F. Gao, Q. Chen, L.M. Peng, Journal of the American Ceramic Society 130 (2008) 1124.
[70] D.R. Baker, P.V. Kamat, Journal of Physical Chemistry C 113 (2009) 17967.
[71] L. Ch Chen, Y.Ch. Ho, W.S. Guo, ChM. Huang, T.Ch. Pan, Electrochimica Acta 54 (2009) 3884.
[72] F. Bonfatti, S. Ferro, F. Lavezzo, M. Malacarne, G. Lodi, A. De Battisti, Journal of the Electrochemical Society 147 (2000) 592.
[73] C.A. Martinez-Huitle, S. Ferro, A. De Battisti, Electrochimica Acta 49 (2004) 4027.
[74] C.A. Martínez-Huitle, S. Ferro, Chemical Society Reviews 35 (2006) 1324.
[75] S. Ferro, C.A. Martínez-Huitle, A. De Battisti, Journal of Applied Electrochemistry 40 (2010) 1779.
[76] C.A. Martínez-Huitle, E. Brillas, Applied Catalysis B: Environmental 87 (2009) 105.